Available online at www.sciencedirect.com

ScienceDirect

Proceedings of the Combustion Institute 35 (2015) 3557–3564

Proceedings of the Combustion Institute

www.elsevier.com/locate/proci

Effect of hydrogen addition on the structure of natural-gas jet-in-hot-coflow flames

L.D. Arteaga Mendez*, M.J. Tummers, E.H. van Veen, D.J.E.M. Roekaerts

Laboratory for Aero & Hydrodynamics, Delft University of Technology, Leeghwaterstraat 21, 2628CA Delft, The Netherlands

Available online 22 July 2014

Abstract

Measurements of the flame luminescence, velocity and temperature were conducted in four flames with different natural-gas/hydrogen fuel mixtures (at similar jet Reynolds numbers) in a jet-in-hot-coflow burner that mimics conditions found in real flameless combustion burners. The results show major changes in the flame stabilization mechanism when the hydrogen content of the fuel is increased. By gradually increasing the hydrogen concentration in the fuel, the typical autoignition kernels observed in natural-gas flames are detected at more upstream positions. At sufficient high hydrogen concentrations, the autoignition kernels are not detectable and the flame zone becomes a single continuous region. Temperatures higher than adiabatic are observed at the stabilization region in the hydrogen containing flames suggesting that preferential diffusion plays an important role in the stabilization mechanism of hydrogen enriched hydrocarbon fuels.

Keywords: Flameless combustion; Hydrogen; Flame stabilization; Jet-in-hot-coflow

1. Introduction

Low pollutants emissions and high thermal efficiencies are achieved in combustion systems operating with flameless oxidation (FLOX) and other similar combustion technologies [1–3]. In these combustion technologies, the exhaust heat is recovered to preheat the reactants and high recirculation rates are used to dilute the reactants prior to combustion reactions [4]. In comparison to conventional combustion, FLOX produces more uniform temperature distributions, much lower NOx emissions and higher thermal efficiency [5,6]. The extension of flameless combustion technologies to non-traditional hydrogen containing fuels (e.g. coke oven gas, blast furnace gas and hydrogen enriched natural gas) can produce important benefits if the typical performance levels obtained with traditional hydrocarbon fuels can be also achieved.

In jet-in-hot-coflow flames, a high-speed turbulent jet issues into a slowly moving coflow of hot

* Corresponding author.
E-mail address: L.D.ArteagaMendez@tudelft.nl (L.D. Arteaga Mendez).

http://dx.doi.org/10.1016/j.proci.2014.06.146
1540-7489/

and lean combustion products. This mimics the exhaust heat recovery and dilution due to intense recirculation rates typically found in clean combustion technologies.

Literature reports on experimental research on several jet-in-hot-coflow burners [7–9] contributed to a better understanding of the stabilization mechanism and structure of these flames. Autoignition was suggested as part of the flame stabilization mechanism for H_2/N_2 and CH_4/Air jet flames [7,10]. Later, autoignition kernels were observed as principal stabilization mechanism in CH_4 and Dutch Natural Gas (DNG) jet flames oxidized in different jet-in-hot coflow burners operating at different conditions [9,11]. The oxygen level in the coflow was found to control the OH distribution and peak mean temperature values in the reaction zone of a CH_4/H_2 jet flame [12]. The OH distribution and peak mean temperatures can be also affected by the amount of hydrogen present in the fuel. A C_2H_4/H_2 jet flame showed higher levels of OH and peak mean temperatures in the reaction zone compared to a pure C_2H_4 flame at equal Reynolds number oxidized under the same coflow conditions [13]. For different hydrocarbon fuels (natural gas, ethylene and LPG) mixed with hydrogen, a similar reaction zone structure is observed regardless the major differences in the combustion properties of each pure hydrocarbon fuel [14]. These results show that hydrogen addition to the fuel significantly affects in the stabilization mechanism and flame structure that are not yet completely understood.

Numerical investigations on flameless combustion and jet-in-hot-coflow burners for both traditional hydrocarbon and hydrogen containing fuels are also reported in the literature. From predictions in well stirred reactors, it was computed that adding small amounts of hydrogen to methane enhances the reactivity of the mixture and the hydrogen oxidation kinetics significantly affect the kinetics of pure methane [15]. Also predictions of temperature and thermal NO_x in CH_4/H_2 mixtures at flameless oxidation conditions in a similar configuration were reported consistent with experimental data [16]. The experimental measurements from [8] were consistently predicted in [17,18] highlighting that the effects of differential diffusion of hydrogen are of major importance. Increasing the hydrogen concentration in the fuel enhances diffusive mixing of fuel and oxidizer [19].

The objective of this work is to determine the effects of gradual hydrogen addition on the stabilization of turbulent jet flames oxidized in a hot and lean mixture similar to the media present in flameless combustion systems. The flame structure transition due to the gradual increase of hydrogen in the fuel composition and its effects in the velocity field and temperature are presented in this paper.

2. Experimental setup

2.1. The Delft jet-in-hot-coflow burner

Figure 1 shows a schematic of the Delft jet-in-hot-coflow (DJHC) burner reported in [9]. It was designed to study the combustion of turbulent jet flames oxidized in a controlled environment with full optical access. The DJHC burner consists of an air cooled fuel pipe with an inner diameter of 4.5 mm that is concentrically aligned inside a larger pipe with an inner diameter of 83 mm. During operation, the larger pipe encloses a stream of hot lean combustion products. This hot coflow is produced by a partially premixed ring burner located at the base of the burner. The temperature and oxygen concentration of the hot coflow are controlled by adjusting the power and fuel-to-air ratio of the partially premixed ring burner. The total length of the DJHC burner is approximately one meter and it is a modified version of the jet-in-hot-coflow burner from Adelaide reported in [8]. The Delft version of the burner allows the use of seeding particles in both the fuel jet and the coflow which is necessary to perform velocity measurements with LDA and/or PIV. All the flows to the DJHC burner are controlled with a set of precision Mass Flow Controllers (Bronkhorst, model EL-FLOW® with ± 0.05% inaccuracy). For the reference system, a coordinate system was chosen with the origin at center of the fuel pipe exit. The radial and axial coordinates are denoted by r and z, respectively.

2.2. Case description and coflow conditions

The base fuel is DNG which has an approximate composition of 81.3% CH_4, 14.3% N_2 and

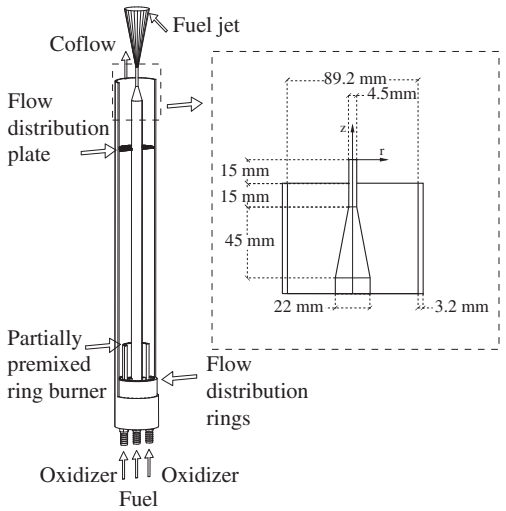

Fig. 1. Schematic of the Delft Jet in Hot-Coflow burner.

2.9% C_2H_6. The remainder mainly consists of higher hydrocarbons. The three other fuel cases (5%H_2, 10%H_2 and 25%H_2) are the result of mixing DNG with hydrogen. The case name reflects the volumetric concentration of hydrogen in the fuel. The operating conditions of the fuel jets are summarized in Table 1. The Reynolds number is based on the diameter of the fuel pipe, the bulk velocity and the kinematic viscosity of the fuel. The latter was calculated using transport properties computed with Cantera software [20] at a temperature of 300 K and a pressure of 1.023 bar. The hot coflow was produced by feeding the partially premixed ring burner with 15.3 nl/min of DNG and 231 nl/min of air.

Figure 2 (top) displays the axial mean velocity component at z = 3 mm. The jet velocity increases with increasing hydrogen content to maintain a (nearly) constant Reynolds number of 5.7×10^3. Figure 2 (bottom) shows that the turbulence intensity I (calculated as $I=\sqrt{\overline{u'u'}+2\overline{v'v'}}/U_0$ with U_0 being the centerline velocity) measured at $z = 3$ mm is similar for all the jets.

The measured mean temperatures in Fig. 3a decrease in the vicinity of the centerline due to heat loss to the relatively cool fuel pipe wall and at the edge of the coflow due to heat loss to the larger pipe. The RMS values of the temperature (Fig. 3b) are constant across the coflow at a level of approximately 120 K. The oxygen concentration measurements at $z = 3$ mm (Fig. 3c) were performed with a commercial Testo 335 flue-gas analyzer. The inaccuracy of the analyzer is ±0.20%. The coflow settings were reproduced from earlier work [21], namely coflow case DJHC-V. For the measurements reported here, a modification in the secondary burner was made, improving the mixing in the coflow stream and thus producing more homogeneous profiles. Species concentrations in the coflow are based on an equilibrium assumption as discussed in [22].

2.3. Experimental techniques

The flame luminescence was recorded by using an intensified camera (Lambert Instruments HICAM CR). A Nikon UV 1:4.5, $f = 105$ mm lens with a spectral transmission of 70% between 220 and 900 nm was used to collect the light. The pixel density is 8.5 pixels/mm for all the measurements and the gate time was set at 400 μs. For the 25%H_2-J1 flame case, additional recordings with a pixel density of 32 pixels/mm and a gate time of 150 μs were also performed. To compute reliable time averaged statistics of the flame luminescence, 10^4 frames were captured at frame rate of 50 Hz.

The velocity field was measured with a PIV system that is based on a high repetition rate Quantronix DarwinDuo 80-M Nd:YLF laser producing light at 527 nm wave length and a Photron SA1 high-speed camera. The laser produces a beam that is converted into a laser sheet of 60 mm height and a thickness of 0.6 mm by three cylindrical lenses. This sheet illuminates alumina particles with a mean diameter of 1 μm that are dispersed in both the coflow and the fuel jet.

Table 1
Operating conditions of the fuel jets where $\dot{m}$ is the mass flow rate, Re is the Reynolds number and P is the power.

Jet flame	$\dot{m}\times10^{-4}$ kg/s	Re –	P kW
DNG-J1	2.51	5700	10.3
5%H_2-J1	2.50	5700	10.4
10%H_2-J1	2.48	5650	10.4
25%H_2-J1	2.44	5550	10.7

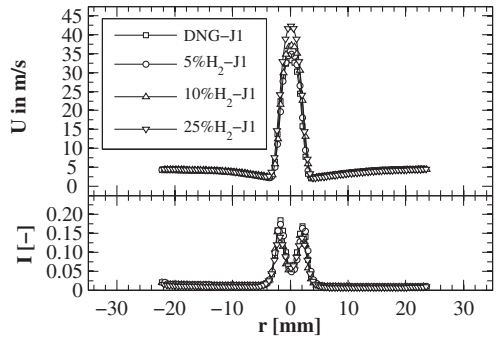

Fig. 2. Inflow boundary conditions for the studied flames measured at $z = 3$ mm. Top: Axial mean velocities measured with PIV. Bottom: turbulence intensity, calculated as $I=\sqrt{\overline{u'u'}+2\overline{v'v'}}/U_0$, with U_0 being the centerline velocity at the nozzle exit.

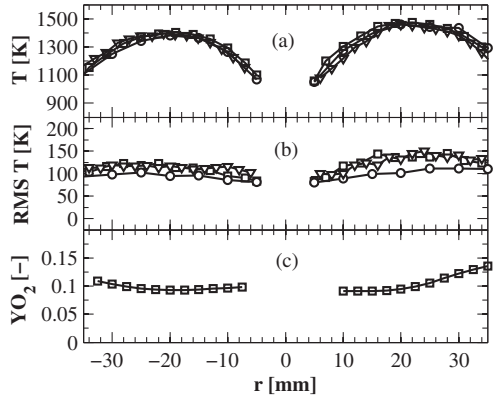

Fig. 3. Inflow boundary conditions for the studied flames measured at $z = 3$ mm. (a) Mean temperatures measured with CARS, (b) Temperature RMS and (c) oxygen mass fractions measured with a flue gas analyzer. Legend as in Fig. 2.

The scattered light is collected by a 105 mm Nikon Nikkor ED lens. To compute the vector fields, Davis 7 software performs two passes over interrogation areas of 32 × 32 pixels followed by three passes over a reduced interrogation area of 16 × 16 pixels. The pixel density is 17 pixels/mm. The statistics were obtained from 4500 image pairs with a time separation of 20 μs in the region near the jet exit and 30 μs farther downstream.

The instantaneous temperatures were measured with a CARS system described in detail in [23]. At each point, 10^3 samples were measured at a sampling rate of 10 Hz. The instantaneous temperatures reported here are obtained from a probe volume with a diameter of 35 μm and a length of 700 μm. The estimated error in each single shot measurement is around 20 K with a variable inaccuracy of 4% at low temperatures (~300 K) and 1% at high temperatures (~2000 K).

3. Results

3.1. Effects on the lift-off height

Figure 4 shows color photos of the four flames taken at two different exposure times. For each flame the photo on the left corresponds to the long exposure time (1 s) while the one of the right corresponds to the short time exposure (0.5 ms). The long exposure time photos clearly show that (as expected) increasing the hydrogen content of the fuel reduces the lift-off height. The short exposure time photos show the transition in the flame stabilization structure. The stabilization zone of the DNG-J1 flame clearly exhibits autoignition kernels that grow while being convected downstream until they merge into a connected flame zone. The behavior of these isolated flame pockets is as the described in [9]. An exemplary image of the autoignition kernels is marked by the red ellipse in Fig. 4 (DNG-J1). The 5%H_2-J1 flame also exhibits autoignition kernels in the stabilization region. In comparison to DNG-J1 flame, these kernels occur in a region with smaller streamwise length that is located closer to the jet exit. The lifetimes of these kernels are much shorter than in the DNG-J1 flame because they rapidly merge to form the connected flame zone. Ignition kernels are not detectable in the 10%H_2-J1 and the 25%H_2-J1 flames, where the flame front appears to be connected at all the time.

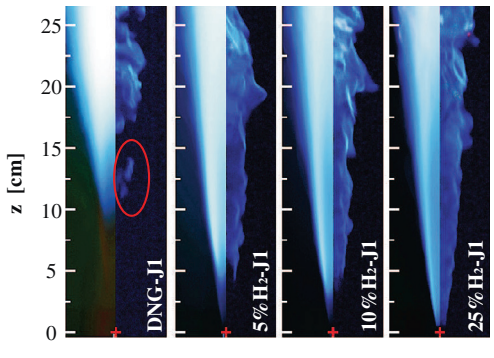

Fig. 4. Images of the flame base taken at a long exposure time of 1 s (left) and a short exposure time of 0.5 ms (right). The red ellipse points out an autoignition kernel and the red crosses denote the fuel pipe exit. The window width is approximately 8 cm. (For interpretation of the references to colour in this figure legend, the reader is referred to the web version of this article.)

Figure 5 shows the mean flame luminescence in the stabilization region for the 25%H_2-J1 flame and three instantaneous snapshots with a separation time of 1 ms. The instantaneous images do not show autoignition kernels and the mixing zone is well separated from the flame zone. The flame zone is a continuous and single region. Sometimes dark spots are observed in the flame zone. These are interpreted as failed ignition regions. The observed structure suggests a change in the stabilization mechanism unless the process of formation of autoignition kernels followed by kernel growth into a connected flame zone takes place in a very short region so that it could not be detected with the current experimental setup. Similar results were reported by Oldenhof et al. [9,21] and Arndt et al. [24] while studying natural gas and methane flames. They reported that increasing the hot coflow temperature shifts the stabilization region upstream and narrows the streamwise region where autoignition kernels are detected. Arndt et al. [24] also reported that at coflow temperatures higher than 1700 K, the autoignition kernels are not detected and the stabilization region shows features similar to those observed in flames stabilized by flame propagation. For pure hydrocarbon fuel jets, increasing the coflow temperature produces a similar effect

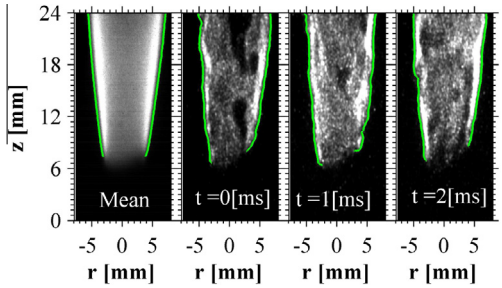

Fig. 5. Mean and three sequential instantaneous flame luminescence images from the 25%H_2-J1 flame. The green line marks the edges of the flame. (For interpretation of the references to colour in this figure legend, the reader is referred to the web version of this article.)

as increasing the hydrogen concentration in the jet fuel while keeping the coflow settings.

In addition to the lift-off height, the edges of the flame (green lines in Fig. 5) were also tracked to determine the radial position of the stabilization point at the lift-off height. The coordinates of stabilization point identified in this way will be used in the next section to have an estimate of the velocity in the flame stabilization point.

Oldenhof et al. [9] introduced the probability of finding a flame at an axial height z on any radial location $P_{b2}(z)$. The lift-off height was then defined as the axial height z where $P_{b2}(z) = 0.5$. Figure 6 shows $P_{b2}(z)$ from the fuel pipe exit at $z = 0$ mm up to $z = 250$ mm for the four flames. $P_{b2}(z)$ was determined here from instantaneous flame luminescence images recorded by the HICAM-CR intensified camera. The addition of hydrogen not only shifts the stabilization region upstream, but it also shortens the stream-wise length of the region where the transition to a continuous flame zone occurs. Additionally, the first luminescence events are also shifted upstream showing that the first combustion reactions are occurring earlier when hydrogen is present in the fuel.

3.2. Effects on the velocity field

Figure 7 compares the streamlines and the turbulence intensity computed from PIV measurements for the four flames. In the coflow region, the streamlines are nearly axial and the velocity has a magnitude of approximately 4 m/s. In the region were the coflow and the jet begin to interact streamlines bend in the direction of the jet due to entrainment of coflow into the fuel jet. Until now, the described features of the velocity field present minor differences among the studied flames.

The color map in Fig. 7 shows the turbulence intensity of the axial velocity, i.e. u'/u. The turbulence intensity is very low in the coflow region and has the highest values in the shear layer region. Increasing the hydrogen concentration in the fuel jet results in regions that can maintain the turbulence intensity levels over longer streamwise regions. This may be caused by the fact that the presence of hydrogen not only triggers ignition

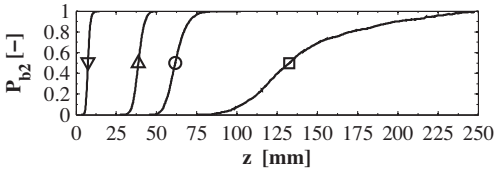

Fig. 6. Probabilities of finding flame luminescence as a function of the height above the fuel nozzle exit (P_{b2}). The symbols (as described in Fig. 2) indicate the location where $P_{b2} = 50\%$ corresponding to the lift-off height.

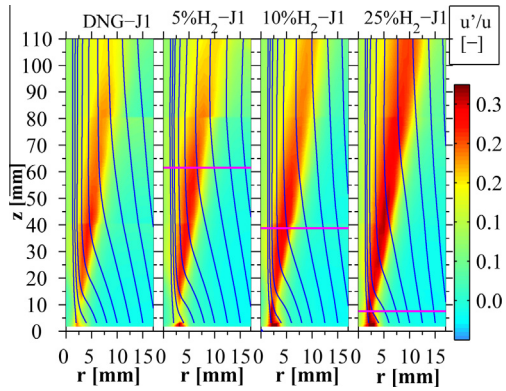

Fig. 7. Color map of turbulence intensity of axial velocity fluctuations (u'/u) levels for the four studied flames. The solid magenta line marks the position where $P_{b2} = 50\%$. The solid blue lines are stream lines. (For interpretation of the references to colour in this figure legend, the reader is referred to the web version of this article.)

at more upstream positions, but it also enables chemical reactions to occur deeper in the turbulent shear layer.

Using the locations of the flame edges at the lift-off height computed for the 25%H_2-J1 (green lines from Fig. 5) the mean axial velocity and turbulence intensity can be extracted at the estimated stabilization points. These points lie in a turbulent region were the mean axial velocity is 3.4 m/s and the turbulence intensity is 30%. This result confirms that in the 25%H_2-J1 flame case, ignition reactions occur in a turbulent region.

3.3. Effects on the temperature field

Figure 8 presents the results of the CARS temperature measurements for the 5%H_2-J1 flame at $z = 65$ mm. This axial station corresponds to the lift-off height for this flame. The mean temperature profile in Fig. 8a shows a steep increase from the centerline to the radial position of $r = 9$ mm. This is the jet region where the sharp temperature gradient is caused by the mixing of the cold fuel with the hot coflow. For higher radial positions, the profile reflects the coflow temperature. At this axial station, the mean temperature profile does not show any evidence of local ignition events while it is known from the flame luminescence measurements (see Fig. 6) that ignition kernels occur regularly.

The 95% Upper Confidence Limit (UCL) of the temperature PDF is a useful instrument to reveal the presence of exothermic reactions due to the ignition kernels. By definition, 97.5% of the measured instantaneous temperatures are below the 95% UCL [25]. The 95% UCL profile in Fig. 8a shows a clear peak at the location where

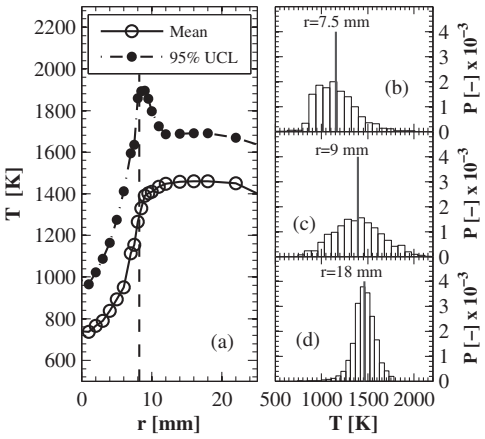

Fig. 8. Measured temperatures for the 5%H_2-J1 flame at $z = 65$ mm. (a) Mean temperature (open circle) and corresponding 95% UCL (filled circle). The vertical dashed line marks the location of peak turbulence intensity. (b)–(d) Temperature PDFs at the indicated radial position. The vertical lines mark the mean temperatures of the PDFs.

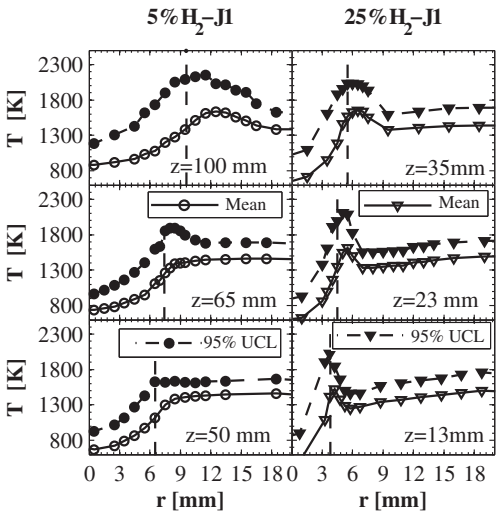

Fig. 9. Mean temperature and corresponding 95% UCLs for the 5%H_2-J1 and 25%H_2-J1 flames in the stabilization region. The dashed line marks the location of peak turbulence intensity.

high instantaneous temperatures caused by ignition kernels occur. The region where temperatures higher than the coflow temperatures exist is located between $r = 7.5$ mm and $r = 12$ mm. Also shown in Fig. 8a is a vertical dashed line at $r = 8$ mm that marks the radial location where the turbulence intensity u'/u has a maximum. The peak of the 95% UCL occurs very close to the turbulence intensity maximum (at $r = 9$ mm) showing that autoignition reactions occur in a turbulent region.

Figure 8b shows a PDF that is measured at a point where ignition reactions are occasionally detected ($r = 7.5$ mm). The PDF shows predominantly low temperatures counterbalancing the effect of the high temperature tail due to the combustion reactions. Figure 8c shows the temperature PDF at a point with the highest ignition reactions frequency. This PDF shows that instantaneous temperatures are distributed over a wide range between 780 and 2100 K. The broad and symmetrical distribution of temperatures produces a mean temperature value that does not reveal the effect of combustion reactions. To compare, Fig. 8d shows a temperature PDF measured at a location in the coflow ($r = 18$ mm) and at the same axial station of $z = 65$ mm. This PDF shows a high kurtosis compared to the other temperature PDFs. The mean temperature profile is thus not a reliable indicator for the occurrence of ignition kernels.

Figure 9 compares temperature profiles for the 5%H_2-J1 and the 25%H_2-J1 flame cases. The three axial stations were selected to capture the flame stabilization region from the most upstream position where ignition reactions are initially detected to an axial station where flame luminescence was always present.

At the axial stations of $z = 100$ mm and $z = 35$ mm the flames are stable and flame luminescence is always present. Both the mean temperature profiles and corresponding 95% UCL show peaks that are attributed to combustion reactions. The high temperatures occur over a wider radial region in the 5%H_2-J1 flame. Compared to the 25%H_2-J1 flame, the radial location of the peak mean temperature is displaced towards larger values of r taking the peak of turbulence intensity as a reference. The increase of hydrogen concentration in the fuel enables combustion reactions at more turbulent regions.

At the intermediate axial stations of $z = 65$ mm and $z = 23$ mm only the 25%H_2-J1 flame has a mean temperature profile reflecting combustion reactions. For the 5%H_2-J1 flame it is necessary to use the 95% UCL of the temperature PDF to identify the combustion reactions. Finally, at the most upstream stations of $z = 50$ mm and $z = 13$ mm, only the 25%H_2-J1 presents peaks in both the mean temperature and the corresponding 95% UCL. These peaks are located in a high turbulence intensity region.

Temperatures above the adiabatic flame temperature (computed with Cantera software [20]) were measured in the hydrogen flames but not in the DNG-J1 flame. The DNG-J1 flame shows temperatures ranging from 870 to 1700 K (discounting 2.5% of the extreme temperatures at each PDF tail) in a temperature PDF located at a point where autoignition events frequently

occur. Assuming an initial mixture temperature of 870 K and computing the stoichiometric adiabatic flame temperature for DNG given the oxidizer composition, the resulting temperature is equal to 1735 K. This temperature is close to the maximum temperatures measured in the temperature PDF.

At the most upstream axial station of $z = 13$ mm, the 25%H_2-J1 flame case presents a temperature PDF with temperatures ranging from 980 to 1925 K (discounting 2.5% of the extreme temperatures at each PDF tail). Assuming an initial mixture temperature of 980 K, the stoichiometric adiabatic flame temperature can be calculated. The dark spots observed in the instantaneous snapshots of flame luminescence (Fig. 5) support the assumption that the un-ignited mixture temperature is close to 980 K. The resulting adiabatic flame temperature given this condition is equal to 1845 K. This computed temperature is 95 K below the observed peak temperatures and a possible explanation for the phenomenon is that the concentration of hydrogen in the point is higher than the original concentration of the supplied fuel. This suggests that besides turbulent mixing, differential diffusion is an important transport mechanism for hydrogen containing flames and also explains the high measured temperatures.

Additional evidence of the effects of differential diffusion can be obtained from the comparison of velocities at the flame base and the burning velocity. Earlier experimental work on conditioned statistics at the flame base of turbulent lifted jet flames [26,27] shows that the upstream velocities are less than $3S_L$ where S_L is the stoichiometric freely propagating flame laminar burning velocity. Table 2 presents calculated laminar burning velocities for DNG and hydrogen mixtures oxidized in the hot coflow at different initial temperatures. The calculations were performed in CHEM1D [28] using the GRI-3.0 chemical mechanism. The visual appearance of the 25%H_2-J1 flame at the flame base resembles an ordinary lifted jet flame with mean velocity of 3.4 m/s at the mean flame base. Assuming that this is the upstream flame velocity, the highest expected S_L should be 1.13 m/s. This value is significantly higher than the calculated 0.83 m/s for the 25%H_2 fuel composition at 1000 K suggesting that the hydrogen concentration of the fuel at the stabilization region is higher than the original 25%.

Table 2
Laminar burning velocities (S_L) of stoichiometric fuel mixtures at three initial temperatures oxidized in hot coflow.

	S_L [m/s]		
	600 [K]	800 [K]	1000 [K]
DNG	0.041	0.198	0.646
25%H_2	0.063	0.265	0.830
50%H_2	0.102	0.399	1.213
75%H_2	0.218	0.812	2.407
100%H_2	1.303	4.245	11.240

4. Conclusions

Measurements of the flame luminescence, velocity field and instantaneous temperatures of four flames with increasing concentration of hydrogen in their fuel composition oxidized in the DJHC burner at similar conditions were presented. The results show that hydrogen is an excellent flame stabilization agent even at hydrogen concentrations in the fuel as low as 5%. The presence of hydrogen changes significantly the flame structure compared to natural-gas flames. These changes include a substantial upstream shift of the stabilization region and the reduction or suppression of autoignition kernels as the principal stabilization mechanism resulting in a behavior similar to that observed in ordinary lifted flames oxidized in air. The high peak temperatures found in flames of hydrogen containing fuels compared to the DNG flame, suggest that besides turbulent mixing also differential diffusion has an important role in the stabilization mechanism when the fuel contains hydrogen. Increasing the hydrogen concentration in the fuel produces a velocity flow field with higher turbulence intensity in the shear layer region.

Acknowledgements

This project is financially supported by the Technology Foundation STW.

References

[1] J.A. Wünning, J.G. Wünning, *Prog. Energy Combust. Sci.* 23 (1) (1997) 81–94.
[2] M. Katsuki, T. Hasegawa, *Proc. Combust. Inst.* 27 (2) (1998) 3135–3146.
[3] A. Cavaliere, M. de Joannon, *Prog. Energy Combust. Sci.* 30 (4) (2004) 329–366.
[4] A. Milani, A. Saponaro, *IFRF Combust. J.* 1 (2001) 1–32.
[5] J. Wünning, Flameless Oxidation, 6th HiTACG Symposium, Essen, Germany, 2005.
[6] A. Milani, J. Wünning, in: N. Syred, A. Khalatov (Eds.), *Advanced Combustion and Aerothermal Technologies, NATO Science for Peace and Security Series C: Environmental Security*, Springer, Netherlands, 2007, pp. 343–352.
[7] R. Cabra, T. Myhrvold, J. Chen, R. Dibble, A. Karpetis, R. Barlow, *Proc. Combust. Inst.* 29 (2) (2002) 1881–1888.
[8] B.B. Dally, A.N. Karpetis, R.S. Barlow, *Proc. Combust. Inst.* 29 (2002) 1147–1154.

[9] E. Oldenhof, M. Tummers, E. van Veen, D. Roekaerts, *Combust. Flame* 157 (6) (2010) 1167–1178.
[10] R. Cabra, J.-Y. Chen, R. Dibble, A. Karpetis, R. Barlow, *Combust. Flame* 143 (4) (2005) 491–506.
[11] R.L. Gordon, A.R. Masri, E. Mastorakos, *Combust. Flame* 155 (12) (2008) 181–195.
[12] P.R. Medwell, P.A. Kalt, B.B. Dally, *Combust. Flame* 148 (12) (2007) 48–61.
[13] P.R. Medwell, P.A. Kalt, B.B. Dally, *Combust. Flame* 152 (12) (2008) 100–113.
[14] P.R. Medwell, B.B. Dally, *Combust. Flame* 159 (10) (2012) 3138–3145.
[15] P. Sabia, M. de Joannon, S. Fierro, A. Tregrossi, A. Cavaliere, *Exp. Therm. Fluid Sci.* 31 (5) (2007) 469–475.
[16] Y. Yu, W. Gaofeng, L. Qizhao, M. Chengbiao, X. Xianjun, *Int. J. Hydrogen Energy* 35 (7) (2010) 2694–2697.
[17] F. Christo, B. Dally, *Combust. Flame* 142 (12) (2005) 117–129.
[18] A. Mardani, S. Tabejamaat, M. Ghamari, *Combust. Theor. Model.* 14 (5) (2010) 747–774.
[19] A. Mardani, S. Tabejamaat, *Int. J. Hydrogen Energy* 35 (2010) 11324–11331.
[20] D. Goodwin, available at <http://code.google.com/p/cantera/>.
[21] E. Oldenhof, M. Tummers, E. van Veen, D. Roekaerts, *Combust. Flame* 158 (8) (2011) 1553–1563.
[22] G.Sarras, M.K.Stoellinger, D. Roekaerts, Transported PDF simulations of the Delft jet-in-hot-coflow burner based on 4D-FGM tabulated chemistry, in: *Proc. 6th European Combustion Meeting* 2013, paper P1-80.
[23] E.H. van Veen, D. Roekaerts, *Appl. Opt.* 44 (32) (2005) 6995–7004.
[24] C.M. Arndt, R. Schießl, J.D. Gounder, W. Meier, M. Aigner, *Proc. Combust. Inst.* 34 (1) (2013) 1483–1490.
[25] G. Bohm, G. Zech, Introduction to Statistics and Data Analysis for Physicists, Hamburg: Deutsches Elektronen Synchrotron, 2010.
[26] L. Muniz, M.G. Mungal, *Combust. Flame* 111 (1997) 16–31.
[27] C. Maurey, A. Cessou, B. Lecordier, D. Stepowski, *Proc. Combust. Inst.* 28 (1) (2000) 545–551.
[28] CHEM1D, A one-dimensional laminar flame code, Eindhoven University of Technology, URL <http://www.combustion.tue.nl/chem1d/>.